SMAR 2017 – Fourth Conference on Smart Monitoring,
Assessment and Rehabilitation of Civil Structures

SMAR 2017

On the pseudoelastic behaviour in a lath martensitic steel under two discrete processes consist of cold rolling and heat treatment

H.R. Koohdar[1], M. Nili-Ahmadabadi[1,2], M. Habibi-Parsa[1,2], H.R. Jafarian[3]

[1]School of Metallurgy and Materials Engineering, College of Engineering, University of Tehran, Tehran, Iran
[2]Center of Excellence for High Performance Materials, School of Metallurgy and Materials Engineering, College of Engineering, University of Tehran, Tehran, Iran
[3]School of Metallurgy and Materials Engineering, Iran University of Science and Technology, Tehran, Iran

In this paper, a ternary Fe-9.6Ni-7.1Mn (at.%) lath martensitic steel was subjected to study the reverse transformation of martensite to austenite under two discrete processes consist of cold rolling and intercritical annealing at 580 °C in the ferritic-austenitic (α+γ) dual phase region for 0.48 ks. Experimental results such as electron back scattering diffraction (EBSD) and atom probe tomography (APT) were used to characterize the reverse transformation. It was found that fine austenite grains by displacive mechanism could be formed under cold rolling. Also, APT study revealed that under intercritical annealing, the reverse transformation takes place through mixed diffusion control mechanism, i.e. controlled by bulk and interface diffusion. Subsequent isothermal ageing after intercritical annealing was performed at 480 °C for 3.6 ks which resulted in the formation of θ-NiMn precipitates. The cyclic tensile test results revealed pseudoelastic behavior of the reversed austenite in the cold rolled sample and intercritically annealed specimen after subsequent ageing.

1 INTRODUCTION

Low cost iron based shape memory alloys (SMAs) such as Fe-Mn-Si and Fe-Ni-Mn-based alloys with good workability, machinability, and weldability have been drawing much attention during the last two decades regarding to their potential application in engineering. They have been considered for a wide variety of structural applications such as damping materials, clamping or coupling devices, pipe joints and rail couplings [1-5]. The pseudoelastic behaviour in these alloys is known to be based on the strain-induced transformation from austenite (fcc) to epsilon martensite (hcp) under loading and its reversion (hcp to fcc) after unloading [2,6-8]. Accurrance the austenite to epsilon martensite transformation depends on the amount of stacking fault energy (SFE) of the alloy [9].

Fe-9.6Ni-7.1Mn (at.%) low carbon lath martensitic steel is an ultrahigh strength steel which is ductile in the solution annealed condition and shows excellent age hardenability [10-12]. In order to observe the pseudoelastic behavior in this alloy, it is necessary to introduce the austenite phase in the martensite matrix by occurring the reverse transformation of martensite to austenite (reverse transformation) [13,14]. Austenite could be induced thermally or displacevly depends on the process is applied on the alloy.

It is important to note that most of the studies on the pseudoelastic behaviour in iron based SMAs have been focused on alloys with an original austenitic microstructure. The aim of the study is to investigate the reverse transformation in Fe-9.6Ni-7.1Mn (at.%) martensitic steel

under two discrete processes consist of cold rolling and intercritical annealing. Furthermore, special attention was paid to study of the pseudoelastic behavior in this alloy under cold rolling, intercritical annealing and subsequent ageing.

2 EXPERIMENTAL MATERIALS AND PROCEDURES

An Fe-9.6Ni-7.1Mn (at.%) low carbon martensitic steel in solution annealed condition was used as starting material. Two specimens were cut from the starting material and then subjected to the 80% cold rolling and intercritical annealing. Intercritical annealing was performed on the solution annealed specimen with 2 mm thickness in a neutralized salt bath at 580 °C, between austenite start (A_s) and finish (A_f) temperatures, for 0.48 ks followed by water quenching. The A_s and A_f temperatures are 570 and 640 °C, respectively. Also, subsequent isothermal ageing treatment was carried out at 480 °C for 3.6 ks on the intercritically annealed specimen in a neutralized salt bath followed by water quenching.
Microstructures were characterized by electron backscatter diffraction (EBSD), atom probe tomography (APT), and transmission electron microscopy (TEM). The pseudoelastic behavior and strain hysteresis of specimens were examined by applying cyclic tensile loading-unloading test at constant speed of 1 mm min^{-1} using an extensometer at room temperature.

3 RESULTS AND DISCUSSION

3.1 Austenite formation under heavy cold rolling

Fig. 1 shows the grain boundary maps superimposed on phase maps for solution annealed and 80% cold rolled specimens. EBSD maps include high angle grain boundaries (HAGBs: $\theta \geq 15°$), low angle grain boundaries (LAGBs: $2 \leq \theta < 15°$) as well as nucleation sites of austenite. In addition, martensite and austenite phases are shown in red and green colors, respectively. The phase map of the solution annealed specimen (Fig. 1(a)) indicates that the microstructure consists of typical lath martensite consisting packet and block as a substructure of lath martensite with high fraction of LAGBs. Fig. 1(b) shows phase map of the 80% cold rolled specimen. Fine austenite and martensite phases are denoted in this figure.

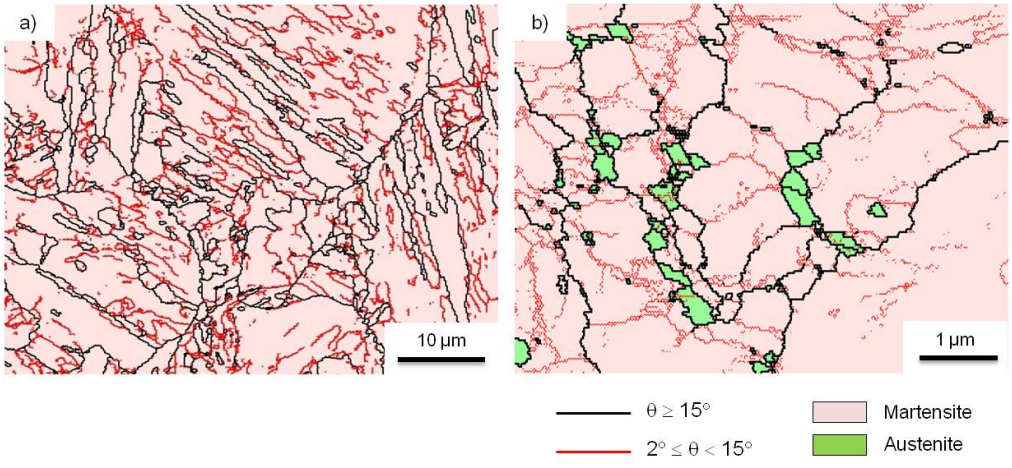

Figure 1. Phase maps of (a) solution annealed, and (b) 80% cold rolled specimens.

It has been reported that during severe deformation at room temperature, austenite can be formed from martensite by displacive mechanism [15]. Deformation in the present study was carried out at room temperature and sample was not heated explicitly therefore, the formation of austenite implies reverse transformation. It has been shown that the austenite reversion is possible even at room temperature if the deformation energy stored in material could provide the required driving force for reverse transformation [16].

3.2 Austenite formation during intercritical annealing

Fig. 2 shows a section of phase map for the intercritically annealed specimen at 580 °C for 0.48 ks. It is obvious that the microstructure consists of reversed austenite and martensite phases.

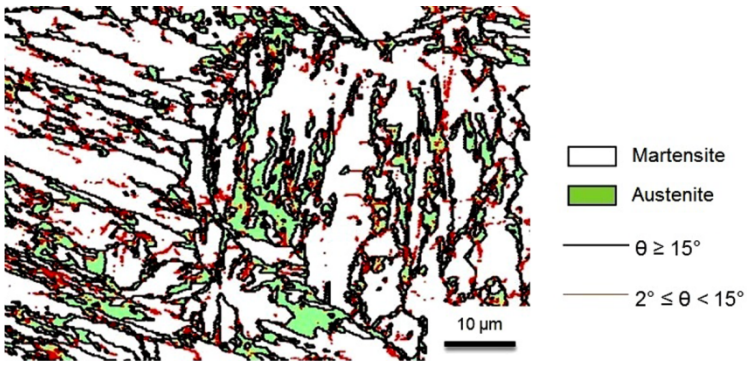

Figure 2. Phase map of the intercritically annealed specimen at 580 °C for 0.48 ks.

The equilibrium phase diagram of the Fe-Ni-Mn alloy at 580 °C calculated by the Thermo-Calc shows that the chemical compositions of martensite and austenite at this temperature are 1.7Ni-0.9Mn and 14.7Ni-11.2Mn (at.%), respectively.

Fig. 3a shows the 3-D atom probe tomography (APT) reconstruction of a martensite-austenite two-phase region in the intercritically annealed specimen. Ni and Mn atoms are respectively displayed in green and red color circles. An interface could be clearly observed through the change in concentration of the Ni and Mn atoms in Fig. 3a. To quantify the concentration of the alloying elements in the martensite and the reversed austenite phases, the area volume selected from the obtained data set was analyzed separately in more details across the martensite/austenite (M/A) interface. A cuboid with the dimensions of ~ 6 × 7 × 21 nm^3 was placed perpendicular to the M/A interface plane (see Fig. 3a) and the concentration profile within the selected volume was integrated and presented along the A-A arrow. Fig. 3b shows the chemical gradients (in at.%) across the martensite-austenite two-phase region in the selected cuboid volume in the direction indicated by the A-A arrow. Also, Fig. 4c represents better resolution of changes in Ni and Mn concentration profile near the M/A interface region (circled area) of Fig. 3b. The concentrations of Ni and Mn elements in the martensite phase close to M/A interface are 5.6 and 2.7 at.%, respectively; and they increase to about 13.1 and 10.9 at.% in the austenite phase. While the nominal bulk composition of the starting material is 9.6Ni-7.1Mn (at.%), the austenite region reveals enrichment and in return the martensite shows depletion of Ni and Mn elements. The enrichment of the reversed austenite by Ni and Mn depicts that the reverse transformation occurred by a diffusional mechanism as reported on other iron-base alloys [17,18].

According to Fig. 3c, the Ni concentration profile perpendicular to the M/A interface is relatively sharper than that of Mn which should be attributed to the lower diffusion coefficient

of Ni in martensite and austenite phases compared with Mn (Table 1). Also, the Mn concentration in austenite near to the M/A interface (10.9 at.%) is close to the value calculated in equilibrium condition at 580 °C by Thermo-Calc (11.2 at.%), whereas for the Ni concentration due to the its lower diffusion coefficient, the real value is totally far from the calculated value. This confirms that the reverse transformation is controlled by the diffusion of Ni element. On the other hand, the concentrations of Ni and Mn elements in martensite near to the M/A interface (5.6Ni-2.7Mn (at.%)) are different from the calculated equilibrium values (1.7Ni-0.9Mn (at.%)) and the difference for Ni is higher than that for Mn due to the lower diffusivity and mobility of Ni in the bulk and interface; therefore, it can be proposed that the reverse transformation during the isothermal heating at 580 °C is mixed diffusion control, i.e. controlled by bulk diffusion and diffusion along the interface.

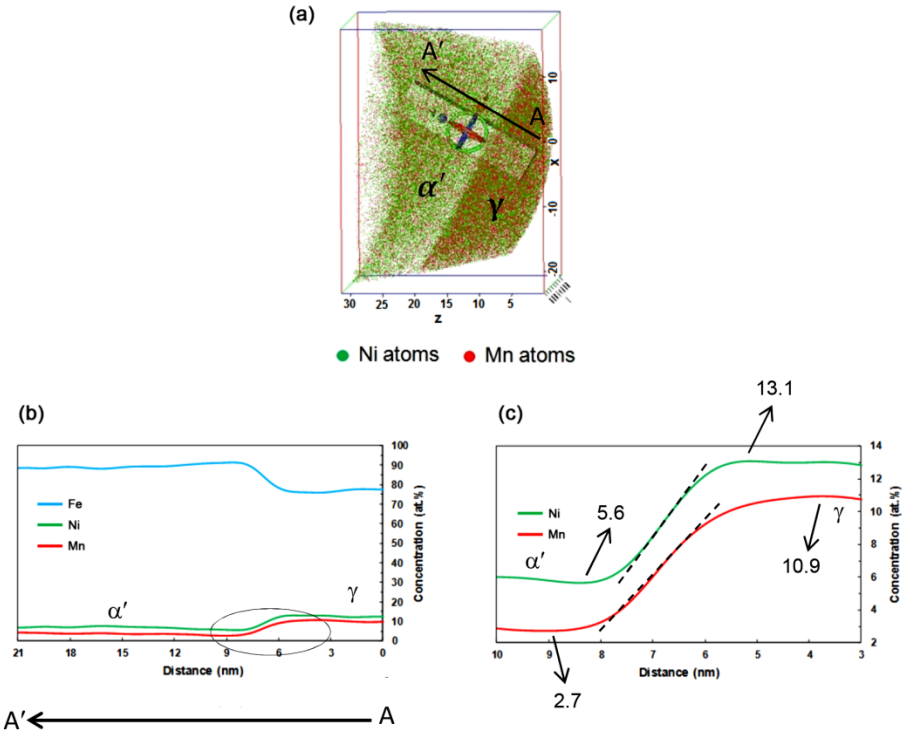

Figure 3. (a) 3-D APT reconstruction of a martensite-austenite two-phase region in the intercritically annealed specimen at 580 °C for 0.48 ks. Ni and Mn atoms are respectively displayed in green and red color circles. (b) Chemical gradients (in at.%) across the martensite-austenite two-phase region in cuboid selected volume in (a) in the direction indicated by the A-A arrow; and (c) the zoomed in on the M/A interface region (circled area) of (b).

Table 1. Diffusion coefficient of Ni and Mn in martensite and austenite phases in iron at 580 °C.

Phase	D_{Ni} (m^2 s^{-1})	D_{Mn} (m^2 s^{-1})
Martensite	1.2×10^{-19}	7.4×10^{-19}
Austenite	5.2×10^{-22}	1.5×10^{-21}

3.3 Subsequent ageing after intercritical annealing

Fig. 4a shows a bright field TEM image of the intercritically annealed specimen after subsequent ageing at 480 °C for 3.6 ks. Also, SAD pattern obtained from θ-NiMn precipitates in martensite (α′) matrix (white circled area) accompanied by key diagram are shown in Figs. 4b and c, respectively. According to the figure, it is clear that the θ-NiMn nano-sized precipitates are formed in the microstructure of intercritically annealed specimen.

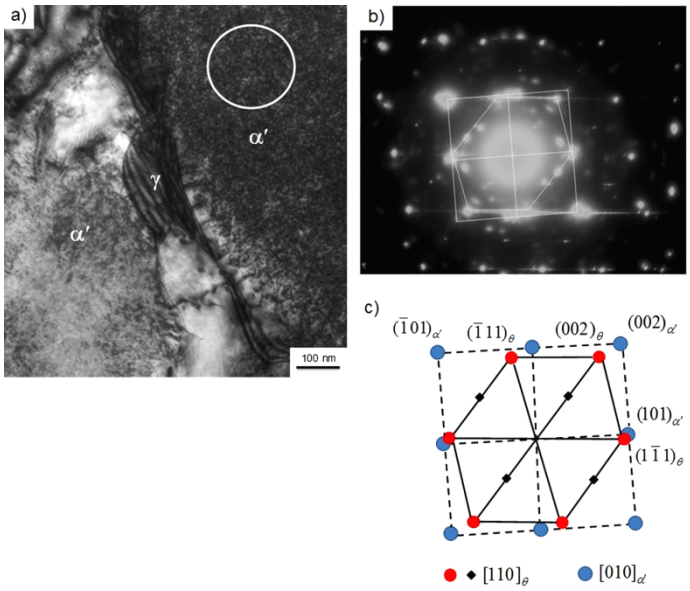

Figure 4. (a) Bright field TEM image of intercritically annealed specimen after subsequent ageing at 480 °C for 3.6 ks showing austenite (γ) and martensite (α′) phases accmpanied by θ-NiMn nano-sized recipitates, (b) SADP obtained from the precipitates in martensite matrix (white circled area); and (c) key diagram related to SADP of the precipitates in martensite matrix.

3.4 Pseudoelastic behavior

Previous studies demonstrated that pseudoelastic behavior in Fe-Ni-Mn steels is related to the austenite (fcc) to epsilon martensite (hcp) transformation under loading and its reversion after unloading [2,19]. Watanabe et al. [2] studied the pseudoelastic behavior in Fe-Ni-Mn SMAs with variety of Ni and Mn content. They found that Fe-5Ni-15Mn alloy has the highest amount of pseudoelasticity which is related to the austenite to epsilon martensite transformation. Later on, Ghasemi et al. [19] found out that austenite to epsilon martensite transformation is the main source of pseudoelasticity in severely deformed Fe-10Ni-7Mn age hardenable martensitic steel. Transformation of austenite to epsilon martensite is induced by gliding of Shockley partial dislocations. In austenite phase, besides the glide of perfect dislocations, other mechanisms of plastic deformation such as mechanical twinning or the formation of epsilon martensite can occur during straining. The plasticity mechanisms depend on the stacking fault energy (SFE). It is reported that SFE lower than 12 mJ m^{-2} is a criterion of austenite to epsilon martensite transformation in iron base alloys [9]. The amount of SFE in the alloy of present study was calculated about 10 mJ m^{-2} by some authors of the present study [20] which indicates this alloy is susceptible to the austenite to epsilon martensite transformation. Their results represented that the austenite can form during cold rolling with stress-induced reverse transformation mechanism and by applying more deformation, e. g. wire drawing, this austenite can transform

to epsilon martensite accompanied by a large density of stacking faults. Therefore, it is expectable to observe the pseudoelastic behavior in this alloy during loading and unloading.

3.4.1 Pseudoelastic behavior after cold rolling

Fig. 5 shows the cyclic stress-strain curves of the solution annealed and 80% cold rolled specimens at room temperature. For solution annealed specimen (Fig. 5(a)), a normal linear elasticity curve without strain hysteresis is only observed since the microstructure of the specimen is fully martensite. According to Fig. 5(b), for the 80% cold rolled specimen, it is obvious that the distinctive feature of the spring back strain is non-linear at the lower stress portion and there is a strain hysteresis between the unloading and reloading curves that increases with increasing applied strain. It seems that the pseudoelastic behavior is attributed to the presence of displacively formed austenite with high dislocation density which promotes fcc to hcp transformation rather than slip during loading-unloading process. In this case, the pseudoelasticity is explained in terms of the reversible motion of the fcc/hcp interfaces if the induced back-stress around the tip of growing martensite plates is taken into account. In the case of the fcc/hcp martensitic transformation, there will be a large pile-up of Shockley partial dislocations with the same sign [21,22]. The accumulation of the dislocations with the same sign produces a large stress field around the tip of the martensite and acts as a back-stress in the growing martensite plate [23].

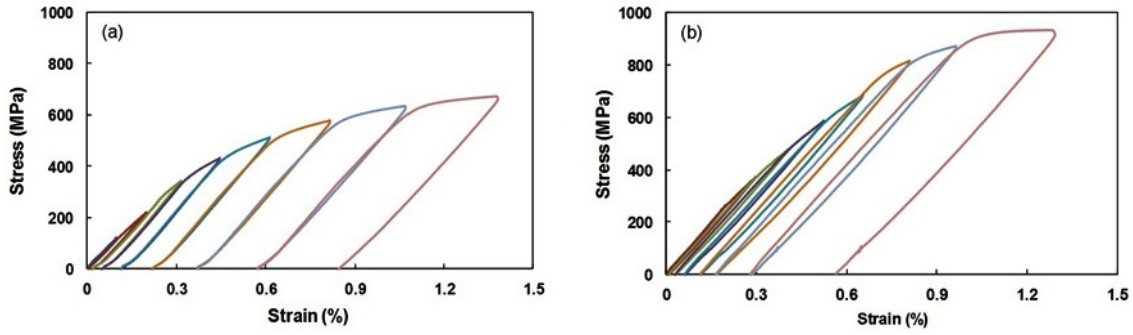

Figure 5. Stress-strain curves of cyclic loading-unloading with increasing strain for (a) solution annealed, and (b) 80% cold rolled specimens.

3.4.2 Pseudoelastic behavior after intercritical annealing and subsequent ageing

The stress-strain curve of cyclic loading-unloading at room temperature for the intercritically annealed specimen at 580 °C for 0.48 has been represented in Fig. 6a. According to the figure, there are no any traces of pseudoelasticity and strain hysteresis. This indicates that slip in the diffusional formed austenite is dominant rather than the strain induced austenite to epsilon martensite transformation. The slip is the main deformation mechanism since the austenite and martensite are soft enough for easy dislocation gliding.

To promote pseudoelasticity, strain induced austenite to epsilon martensite transformation is necessary instead of slip which means austenite strengthening should be considered. It is well known that precipitation hardening is one of the austenite strengthening method [24-26]. Fig. 6b shows the stress-strain curve of cyclic loading-unloading at room temperature for the intercritically annealed specimen followed by subsequent ageing at 480 °C for 3.6 ks. It is apparent that the distinctive feature of the spring back strain is nonlinear at the lower stress

portion, and furthermore, there is obviously hysteresis between the unloading and reloading curves. Also, the strain hysteresis increases with increasing applied strain for all cases. It seems that the pseudoelastic behavior is ascribed to the strengthening of θ-NiMn nano-sized precipitates, as they effectively inhibit the slip deformation. In fact, uniform dispersion of nano-sized precipitates happenes by subsequent ageing and improves the pseudoelastic behavior by strengthening the austenite phase and assisting the reversible movement of the austenite/epsilon martensite (fcc/hcp) interface through a specific crystallographic path [27,28]. One of the reasons could be the back stress on the growing martensite plate caused by the coherent stress field produced by θ-NiMn precipitates. It is important to note that the stress-induced martensite has different equivalent crystallographic routes for returning to the austenite. In order to realize the reversible deformation the return path must be the same as the forward martensitic transformation path [29]. Further research by means of high-resolution TEM observations is needed to clarify the interaction between θ-NiMn precipitates and epsilon martensite in this alloy.

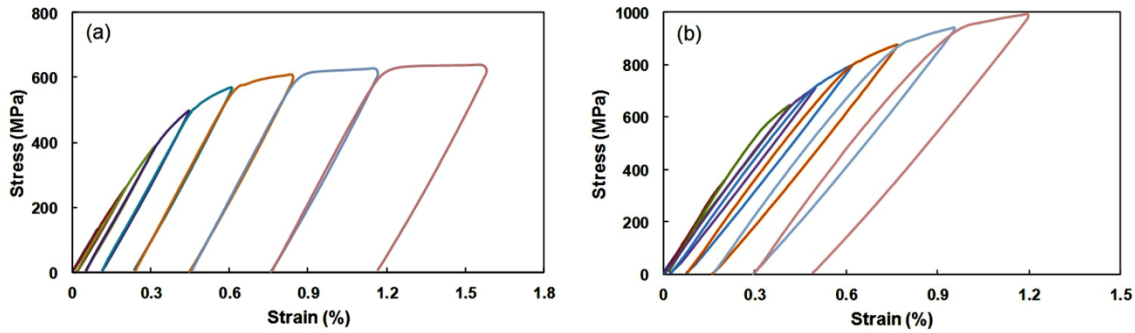

Figure 6. Stress-strain curves of cyclic loading-unloading with increasing strain for (a) intercritically annealed specimen at 580 °C for 0.48 ks, and (b) intercritically annealed specimen after subsequent ageing at 480 °C for 3.6 ks.

4 CONCLUSIONS

In this research, the reverse transformation in Fe-9.6Ni-7.1Mn (at.%) martensitic steel was investigated under two discrete processes consist of cold rolling and intercritical annealing treatment. Furthermore, special attention was paid to study of the pseudoelastic behavior in this alloy under cold rolling, intercritical annealing and subsequent ageing. The main results are summarized as follows;

- EBSD observations showed that the reverse transformation occurs by displacive mechanism after 80 % cold rolling which means the deformation energy stored in the material can provide the driving force required for the reverse transformation. Diformation induced reversed austenite leads to resulting pseudoelasticity in the cold rolled specimen.
- The EBSD and APT results exhibited that austenite formation under intercrtical annealing at 580 °C for 0.48 ks was carried out by mixed diffusion control mechanism, i.e. controlled by bulk diffusion and diffusion along the interface.
- It was found that subsequent isothermal ageing can introduce θ-NiMn nano-sized precipitates in the intercritically annealed specimen. This phenomenon improves the pseudoelastic bahavior by strengthening the austenite and assisting the reversible movement of the austenite/epsilon martensite (fcc/hcp) interface through a specific crystallographic path.

5 REFERENCES

[1] Otsuka, k., A. Saxena, J. Deng, X. Ren, *Philos. Mag.*, 91 (2011) 4514.
[2] Watanabe, S., S. Sato, K. Miura, *J. Mater. Process. Technol.*, 53 (1995) 467.
[3] Dong, Z., UE. Klotz, C. Leinenbach, A. Bergamini, C. Czaderski, M. Motavalli, *Adv. Eng. Mater.*, 11 (2009) 40.
[4] Leinenbach, C., H. Kramer, C. Bernhard, D. Eifler, *Adv. Eng. Mater.*, 14 (2012) 62.
[5] Lee, WJ., B. Weber, G. Feltrin, C. Czaderski, M. Motavalli, C. Leinenbach, *Mater. Sci. Eng. A*, 581 (2013) 1.
[6] Sawaguchi, T., T. Kikuchi, S. Kajiwara, *Smart Mater. Struct.*, 14 (2005) S317.
[7] Lin, HC., SK. Wu, YT. Peng, TC. Cheng, KM. Lin, *J. Alloys Compd.*, 577 (2013) S338.
[8] Baruj, A., G. Bertolino, HE. Troiani, *J. Alloys Compd.*, 502 (2010) 54.
[9] Cabanas Poy, N., Compositional effects on Structure-Property relationships in Mn-based austenitic ferrous alloys. *PhD Thesis*, Ghent University, 2004.
[10] Hossein Nedjad, S., M. Nili Ahmadabadi, T. Furuhara, T. Maki, *Phys. Stat. Sol. A*, 203 (2006) 2229.
[11] Hossein Nedjad, S., M. Nili Ahmadabadi, T. Furuhara, *Metall. Mater. Trans. A*, 39 (2008) 19.
[12] Hossein Nedjad, S., M. Nili Ahmadabadi, T. Furuhara, *Mater. Sci. Eng. A*, 490 (2008) 105.
[13] Koohdar, HR., M. Nili Ahmadabadi, M. Habibi-Parsa, HR. Jafarian, *Mater. Sci. Eng. A*, 621 (2015) 52.
[14] Koohdar, HR., M. Nili Ahmadabadi, M. Habibi-Parsa, HR. Jafarian, H. Ghasemi-Nanesa, H. Shirazi, *Mater. Sci. Eng. A*, 658 (2016) 86.
[15] Allain, S., JP. Chateau, O. Bouaziz, S. Migot, N. Guelton, *Mater. Sci. Eng. A*, 387-389 (2004) 158.
[16] Ghasemi-Nanesa, H., M. Nili-Ahmadabadi, HR. Koohdar, M. Habibi-Parsa, S. Hossein Nedjad, S. A. Alidokht, T. G. Langdon, *Phil. Mag.*, 94 (2014) 1493.
[17] Zel'dovich, VI., Met. Sci. Heat. Treat., 50 (2008) 442.
[18] Nakada, N., T. Tsuchiyama, S. Takaki, S. Hashizume, *ISIJ Int.*, 47 (2007) 1527.
[19] Ghasemi-Nanesa, H., M. Nili-Ahmadabad, H. Shirazi, S. Hossein Nedjad, *TMS annual metting*, USA, 2010.
[20] Ghasemi-Nanesa, H., M. Nili-Ahmadabadi, H. Shirazi, S. Hossein Nedjad, SH. Pishbin, *Mater. Sci. Eng. A*, 527 (2010) 7552.
[21] Liu, DZ., S. Kajiwara, T. Kikuchi, N. Shinya, *Phil. Mag.*, 83 (2003) 2875.
[22] Bergeon, N., G. Guenin, C. Esnouf, *Mater. Sci. Eng. A*, 242 (1998) 77.
[23] Bergeon, N., G. Guenin, C. Esnouf, *Mater. Sci. Eng. A*, 242 (1998) 87.
[24] Kajiwara, S, D. Liu, T. Kikuchi, N. Shinya, *Scr. Mater.*, 44 (2001) 2809.
[25] Stanford, N. and DP. Dunne, *Mater. Sci. Eng. A*, 454 (2007) 407.
[26] Dong, Z., UE. Klotz, C. Leinenbach, A. Bergamini, C. Czaderski, M. Motavalli, *Adv. Eng. Mater.*, 11 (2009) 40.
[27] Baruj, A., T. Kikuchi, S. Kajiwara, *Mater. Sci. Eng. A*, 378 (2004) 337.
[28] Baruj, A., T. Kikuchi, S. Kajiwara, N. Shinya, *Mater. Sci. Eng. A*, 378 (2004) 333.
[29] Sawaguchi, T., T. Kikuchi, S. Kajiwara, Smart Mater. Struct., 14 (2005) S317.